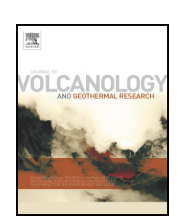
EL SEVIER

Contents lists available at ScienceDirect

Journal of Volcanology and Geothermal Research

journal homepage: www.elsevier.com/locate/jvolgeores



Hydrothermal discharge from the El Tatio basin, Atacama, Chile

Check for updates

Carolina Munoz-Saez a,*, Michael Manga b, Shaul Hurwitz c

- a Centro de Excelencia en Geotermia de los Andes (CEGA), Departamento de Geologia, FCFM, Universidad de Chile, Plaza Ercilla 803, Santiago, Chile
- ^b Department of Earth and Planetary Science, University of California, Berkeley, CA 94720, United States of America
- ^c US Geological Survey, Menlo Park, CA 94025, United States of America

ARTICLE INFO

Article history: Received 27 April 2018 Received in revised form 18 July 2018 Accepted 18 July 2018 Available online 19 July 2018

Keywords: Geothermal Hydrogeology Stable isotopes Chloride inventory Phase separation Geyser

ABSTRACT

El Tatio in northern Chile is one of the best-studied geothermal fields in South America. However, there remain open questions about the mass and energy budgets, water recharge rates and residence time in the subsurface, origin of dissolved solutes, and processes affecting the phase and chemical composition of groundwater and surface water. We measured and sampled surface manifestations of the geothermal system (geysers, perpetual spouters, mud pools/volcanoes, and non-eruptive hot springs) and meteoric water. From the isotopic composition we infer that the thermal water has a meteoric origin that is different from the composition of local meteoric water. The absence of detectable tritium in thermal waters indicates that most of the recharge occurred pre-1950. Boiling and steam separation from the deep reservoir appear to be the main subsurface processes affecting the thermal fluids. A large amount of heat is lost to the atmosphere by evaporation from surface water and by steam emitted from erupting geysers. Using the chloride inventory method, we estimate thermal water discharge to be 218 to 234 L/s, and the advective heat flow to be 120 to 170 MW.

© 2018 Elsevier B.V. All rights reserved.

1. Introduction

The El Tatio geothermal Basin is located in the northern Chilean Andes at >4200 m above sea level (Fig. 1a). It is the one of the largest and best-studied geothermal fields in South America with >200 thermal features within an area of ~30 km² (e.g., Zeil, 1959; Trujillo, 1969; Glennon and Pfaff, 2003; Tassi et al., 2005). It is one of the largest geyser fields in the world (Hurwitz and Manga, 2017), and one of the main tourist attractions in the Atacama region.

Exploration and deep drilling in El Tatio have been conducted sporadically during the 1960s, 1970s, and late 2000s to constrain the conditions of the undeveloped geothermal reservoir (e.g., Healy and Hochstein, 1973; Cusicanqui et al., 1975; Lahsen, 1976a,b; Giggenbach, 1978; Cortecci et al., 2005; Tassi et al., 2005). However, heat flow measurements have not been performed since the 1970s. These earlier data estimated natural hydrothermal discharge of 250 L/s to 500 L/s (Navarro, 1972; Trujillo, 1974) and heat flow between 100 MW to 250 MW (e.g., Mahon, 1970, 1972; Hochstein, 1971; Trujillo, 1974; Muñoz and Hamza, 1993).

The main goals of our study were to estimate the mass and heat budget of El Tatio by combining new measurements with those performed >40 years ago. We also aim to constrain the origin of water recharging the thermal reservoirs and the residence time of groundwater to

E-mail addresses: caromuno@ing.uchile.cl (C. Munoz-Saez), manga@seismo.berkeley.edu (M. Manga), shaulh@usgs.gov (S. Hurwitz).

improve the conceptual model of the geothermal system (e.g. Giggenbach, 1978; Lahsen and Trujillo, 1975). In order to assess the mass and heat budget of the geothermal field, we apply the chloride inventory method (e.g., Ellis and Wilson, 1955; Sorey and Lewis, 1976; Ingebritsen et al., 1989, 2001) and we estimate the enthalpy of the system from the temperature of the reservoir (e.g. Hurwitz et al., 2012). We also performed an experiment to measure the magnitude of heat released by an erupting geyser. To constrain the origin of the recharge of water, we obtained a large data set of oxygen and hydrogen stable isotopes values and augmented with new tritium values of thermal waters. We first describe and discuss the El Tatio geothermal field and the chemical measurements and then present heat flow calculations. We end by synthesizing the new and previous datasets and propose a conceptual model for the geothermal system connecting the local basins to a regional system. These new data and the quantitative analysis can provide land managers and policymakers with the information required to protect this unique natural system and guide possible geothermal exploration in the surrounding area.

2. Geological and hydrothermal background

Most of the thermal features in El Tatio are clustered in three basins (Glennon and Pfaff, 2003): upper basin (UB), middle basin (MB), and lower basin (LB) (Fig. 1b). In this study, we also refer to the mud pools in the north of the UB as Vega Rinconada (VR), the mud pools and mud volcano area south of the MB named the South-East (SE), and thermal features located toward the south of the LB as El Tatio

^{*} Corresponding author.

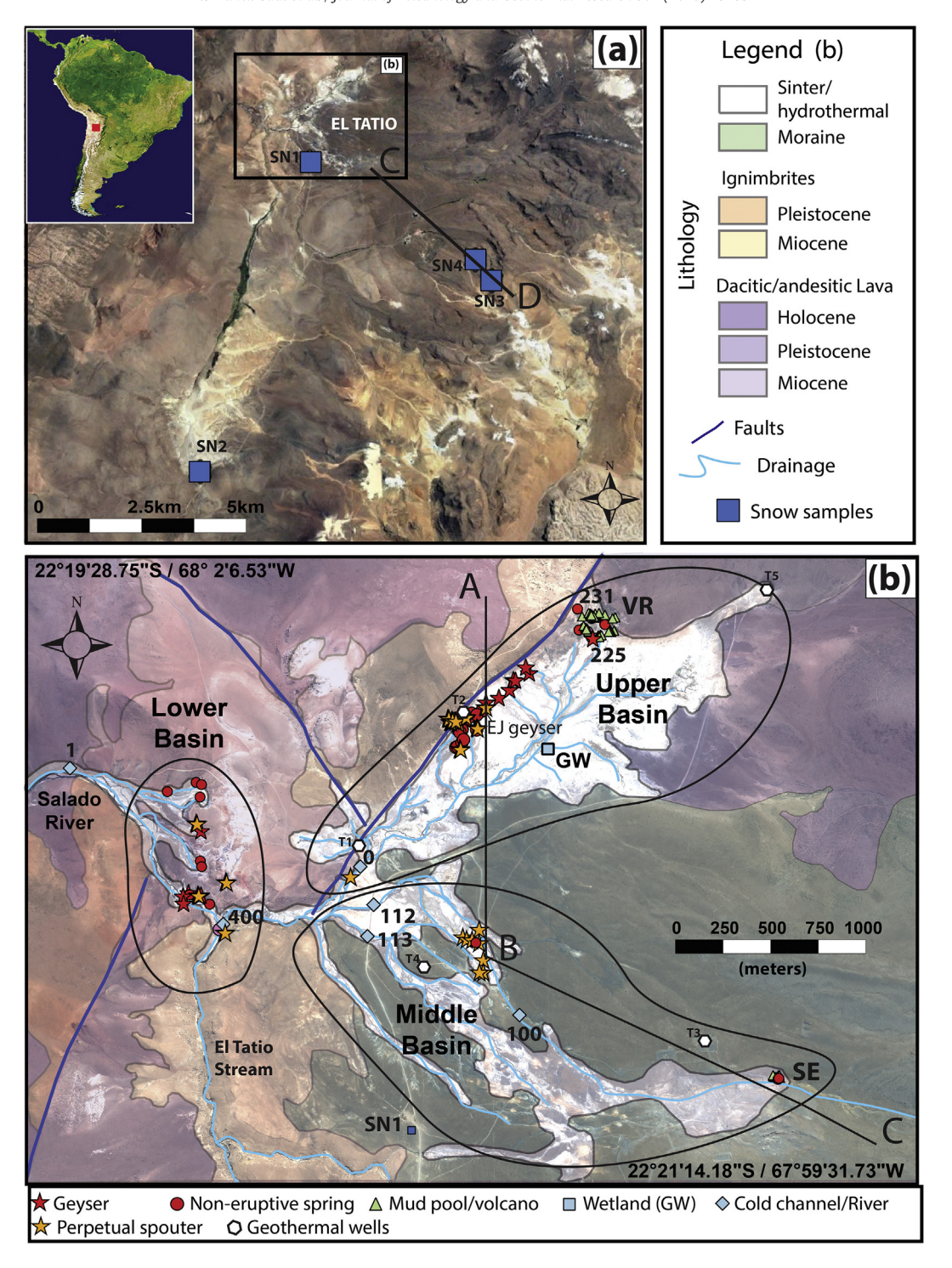


Fig. 1. (a) Aerial photograph of El Tatio geothermal area. Blue boxes are the sites for snow samples SN1, SN2, SN3 and a channel fed by snow melt SN4. (b) Geology of El Tatio geothermal field (modified from Marinovic and Lahsen, 1984). Stars represent eruptive features, red symbols are geysers and yellow symbols are for perpetual spouters. Red circles show the locations of non-eruptive hot springs, blue squares – locations of meteoric water samples, blue diamonds - samples collected in streams, green triangles – mud volcano or mud pool samples, and white hexagons show the location of geothermal wells (Giggenbach, 1978). We labeled sites sampled for the analysis major elements: GW water from wetland, #0 drainage from the Upper Basin and Vega Rinconada (VR), #1 Salado River, #100 drainage from the South East (SE), #122 and #113 are drainages from the Middle Basin (MB), and #400 is discharge in the El Tatio Stream. Coordinates conform to the Universal Transverse of Mercator System (UTM), Datum WGS 84, and Zone 19S. Line C-D in part (a) and A-B-C in (b) are for the cross section presented in Fig. 7.

stream (TS). The UB has the highest concentration of thermal features, which are aligned along the hanging wall of a normal fault defining "the El Tatio half graben" (Lahsen, 1976a,b; Marinovic and Lahsen, 1984). It was proposed that the heat for the system is provided by Holocene andesitic stratovolcanoes that had no historical eruptions (Lahsen, 1976a,b). The geological map (Fig. 1b) indicates that

hydrothermal deposits occur on top of Miocene to Holocene sequences of lavas and ignimbrites and glacial deposits (Marinovic and Lahsen, 1984).

Unpublished data from 1970s suggested that natural thermal discharge of the Rio Salado, which drains the El Tatio geothermal field (Salado River; Fig. 1b) was between 250 L/s in the dry season (Trujillo,

1974) and 400 to 500 L/s during the wet season (Navarro, 1972). Heat flow estimates ranged between 109 MW (Hochstein, 1971) and 209 MW (Trujillo, 1974), based on measurements of direct heat lost from thermal water discharge (Lahsen and Trujillo, 1975). Chloride flux measurements implied a heat flow of 251 MW in wet periods (Mahon, 1970), and 105 to 117 MW in dry and warm periods (Mahon, 1970, 1972). Muñoz and Hamza (1993) recalculated an advective heat flow of 203 MW based on measurements of volumetric flow rates and water chemistry that were published in the 1970s.

Geothermal wells drilled between 1960 and 1970 identified two permeable zones (Lahsen and Trujillo, 1975) associated with two thermal reservoirs (e.g. Cusicanqui et al., 1975; Healy and Hochstein, 1973; Giggenbach, 1978): A, a deeper (>600 m) hotter reservoir (260 to 270 °C), and B, a shallower (<250 m), cooler (160 to 170 °C) and more dilute reservoir. The isotopic compositions of the thermal waters in wells (Giggenbach, 1978) and at the surface (e.g., Ellis, 1969; Giggenbach, 1978; Tassi et al., 2005) led to two contrasting interpretations of the data: (1) thermal water whose composition is determined by rockwater interacction mixed with local meteoric water (Giggenbach, 1978), and/or (2) mixing of meteoric and magmatic waters (Cortecci et al., 2005; Tassi et al., 2005; Tassi et al., 2010). Both interpretations invoked two different isotopic compositions of the meteoric end members for the recharged water.

Hydrogeological models proposed that meteoric waters are recharged through deep faults at higher altitude ~15 to 20 km to the east of El Tatio (e.g., Healy and Hochstein, 1973; Cusicanqui et al., 1975; Giggenbach, 1978; Muñoz and Hamza, 1993) and are then heated along the flow path (e.g., Healy and Hochstein, 1973; Lahsen, 1976a,b). Geophysical surveys identified a zone of low electrical resistivity that extends toward the south and southeast of the field (Lahsen and Trujillo, 1975), suggesting groundwater flow into the basin from that direction. However, precipitation on high-elevation mountains (>5000 m) around El Tatio had not been sampled. One preliminary tritium datum of 3.2 TU (1 TU is equal to 1 atom of ³H per 10¹⁸ atoms of hydrogen) in the water from a geothermal well suggested that meteoric water infiltrates the geothermal reservoir in 10 to 17 years, implying a mean flow velocity of 1 to 1.3 km/year (Cusicangui et al., 1975; Muñoz and Hamza, 1993). In contrast, the original report (Mahon, 1974) suggested there was mixing between two waters, old reservoir water with much younger meteoric water. A more recent study found no tritium in high chloride thermal water (Cortecci et al., 2005).

3. Methods

In October 2014, we collected water samples from two thermal discharges (geyser # 225, and pool # 231 in Table 1), six discharge channels, and from a wetland of slow flowing water (Fig. 1b) for major element chemistry analysis. In April 2017, we collected four additional samples of snow and water from snowmelt channels at elevations of 4200 to 5122 m. Snow samples were melted and filtered in-situ. Samples for major element chemistry were filtered in the field (0.45 µm) and the samples for cation analysis were then acidified with nitric acid. Chemical analysis was carried out approximately one month after sampling at the U.S. Geological Survey water geochemistry laboratories in Menlo Park, California. Concentrations of anions were determined using a Dionex ICS-2000 ion chromatograph with an analytical error of <3% for Cl⁻, F⁻, and SO₄²⁻ and <5% for Br⁻. Total alkalinity as HCO₃⁻ was measured by titrating 10 mL of sample with 0.05 M sulfuric acid to the bicarbonate end-point with an analytical error of ~5%. The concentrations of the major cations were measured using a ThermoFisher ICAP 6000 inductively coupled argon plasma optical emission spectrometer.

The analytical errors for Na $^+$, K $^+$, and B $^+$ are <5%, and for SiO $_2$, Mg $^{2+}$ and Ca $^{2+}$ errors are <10%. The charge imbalance of most samples was \leq 5%, but the relatively large imbalance of a few samples (10–13%) might be a result of either very low ion concentrations (sample #231)

Concentration of major elements.

#	(°C) (mS/	cm)	CI (mg/L)	F ⁻ (mg/L)	Br ⁻ (mg/L)	SO ₄ (mg/L)	HCO_3^- (mg/L)	Ca ²⁺ (mg/L)	(mg/L)	K (mg/L)	Mg ²⁺ (mg/L)	Li ⁺ (mg/L)	Kb (mg/L)	Sr ²⁺ (mg/L)	Ba ²⁺ (mg/L)	Al ⁺ (<) (mg/L)	As ⁺² (mg/L)	SiO ₂ (mg/L)	B (mg/L)	Charge imbalance (%)
0 3	36.3 7.40		050	1.10	3.00	47.5	145	128	1970	218	7.57	17.5	2.91	1.92	0.17	0.07	19.16	204	83.6	12.9
1.	30.5 8.20		3350	1.20	3.20	81.0	180	148	2030	180	12.4	17.5	2.55	2.18	0.18	0.07	20.68	191	87.1	5.46
			400	2.70	5.50	53.0	164	243	3240	155	10.8	27.8	2.65	3.53	0.11	0.12	31.85	210	139	4.25
112 2	23.8 13.9		400	3.80	7.60	0.89	53.0	354	4330	223	99.5	36.5	3.94	5.21	0.18	0.20	42.82	234	191	3.70
			100	4.30	8.30	77.0	57.0	374	4650	236	06.9	39.0	4.16	5.62	0.18	0.20	45.50	250	206	1.70
			540	0.52	1.50	117	271	92.4	961	92.9	20.6	8.34	1.00	1.06	0.21	0.04	11.58	219	41.3	3.57
	35.7 3.80		40	0.27	0.30	41.0	167	19.9	271	30.7	7.20	2.29	0.32	0.22	0.04	0.01	2.82	147	9.2	10.2
	35.6 15.5		000	3.60	8.10	45.0	49.0	290	4600	298	0.62	42.7	8.12	4.80	0.20	0.20	47.43	319	206	4.61
	77.3 0.22		.95	0.10	3.00	22.0	44.0	7.13	20.1	2.95	0.43	0.02	0.01	60.0	0.01	0.01	0.13	142	0.71	11.1
	>0.0 0.0		.01	0.01	1	88.9	ı	1	ı	1	ı	ı	ı	ı	ı	ı	1	ı	ı	ı
	<0.0 0.00		0.02	60.0	1	73.5	ı	1	ı	1	ı	ı	ı	ı	ı	ı	1	ı	ı	ı
SN4 0	0.00 00.00		.02	0.02	1	3.12	1	,	1	1	1	1	1	1	1	ı	1	1	1	ı

or CO₂ degassing between sampling and analysis approximately one month later (samples #0 and GW) (Table 1).

For δ^{18} O and δ D analysis of thermal waters, we sampled catchment channels downstream of the thermal basins and a wetland (sample GW) (Fig. 1b). 60 mL of unfiltered water were analyzed using the water–CO₂ equilibration method for oxygen (Epstein and Mayeda, 1953) and the zinc-reduction method for deuterium (Coleman et al., 1982) at the University of California at Berkeley. Results are reported in delta notation per mil, using the standard reference Vienna-Standard Mean Ocean Water (V-SMOW). The analytical errors for δ^{18} O are ~0.2% and for δ D are ~1%.

For tritium (³H) analysis we collected 500 mL of unfiltered water from discharge streams, from a wetland (GW), and from a thermal spring (# 225 in Table 2). Tritium concentrations were measured using the ³He in-growth method (Bayer et al., 1989) at the U.S. Geological Survey Noble Gas laboratory in Denver, Colorado. About 170 mL of unfiltered water was degassed, sealed in a vacuum flask, and stored for approximately 3 months to accumulate ³He (from the decay of ³H). The concentration of ³He was measured by a magnetic mass spectrometer and was calculated from the storage time and the decay constant (Lucas and Unterweger, 2000), a process that has a detection limit of 0.05 TU.

Water discharge was measured in catchment channels downstream of the thermal basins using a Global Flow probe FP211 with an accuracy of 0.03 m/s. Discharge was calculated by surveying the cross section of the channel and measuring velocity across the channel following standard gauging procedures (Corbett, 1943). We estimate the uncertainty of the discharge values to be about 15% of the measured value.

We calculate thermal water discharge and advective heat output from the El Tatio basin using the chloride inventory method (Ellis and Wilson, 1955), assuming that all the chloride discharged by rivers is derived from the thermal sources within the basin. This assumption is consistent with the very low chloride concentrations of snowmelt upstream of El Tatio (Table 1, samples SN1 to SN4). From the discharge measurements downstream of every basin (Q_S) and the chloride concentration (Cl_S), we calculate the mass flow rate (Q_T) of a group of thermal springs: $Q_T = \frac{Q_S \ (Cl_S - Cl_0)}{(Cl_T - Cl_0)}$. The value Cl_u corresponds to the chloride upstream of every basin, Cl_T is the chloride concentration of a thermal basin, determined from hot spring data, and Cl_0 is the background Cl that we assume to be zero (the value of the snow).

4. Results

The concentrations of Cl $^-$ and Na $^+$ are more than one order of magnitude higher than the concentrations of other major elements dissolved in the thermal waters (Table 1, Supplementary Fig. S1). The electrical conductivity increases linearly with the concentrations of chloride ($\rm r^2 > 0.93$), allowing us to use it as a proxy for salinity. Based on the concentrations of Cl $^-$, SO $_4^2$ and HCO $_3$, we found two distinct end members of thermal waters: water from geyser # 225 (Table 1) corresponds to mature high chloride geothermal water and water from thermal pool # 231 with a low Cl $^-$ concentration is consistent with immature peripheral water. Those two end members are similar to those reported in previous studies (e.g. Giggenbach, 1978; Cortecci et al., 2005; Tassi et al., 2005). There is >10% of imbalance in the charges between anions and cations in some samples from the UB and VR (Table 1, samples # 0, # 231, GW).

Consistent with previous studies (e.g. Giggenbach, 1978; Cortecci et al., 2005; Tassi et al., 2005), we find that waters from erupting geysers have a restricted range of temperature, pH and salinity and their isotopic compositions are similar (Fig. 2, Table 2, Supplementary material Table S1, Fig. S2). They have the highest temperatures, at or a few degrees below the local boiling temperature (86.6 °C), are more saline (especially thermal waters of the UB), and their pH is close to neutral. In contrast, waters from non-eruptive thermal features are more variable; their temperatures are below boiling, their pH can be as low as 5, they are typically less saline, and their isotopic compositions span a wide range of values. In MB, LB and TS water salinities are slightly lower, with respect to those measured in the UB thermal water, but still high enough to be considered mature high chloride thermal waters.

Most of the sampled thermal features are enriched in δ^{18} O with respect to local meteoric water (Figs. 2, 3, Table 2, Supplementary material Table S1, Appendix A), consistent with previous studies (e.g., Giggenbach and Stewart, 1982; Cortecci et al., 2005). Meteoric waters were sampled at different elevations spanning nearly 1 km (4200–5122 m) and there is no clear relationship between isotopic composition and elevation. All meteoric water samples plot on the local meteoric water line (Fig. 3) defined for this part of the Andes (Aravena et al., 1999; Chaffaut et al., 1998). Snow sample SN3 (Fig. 2), was collected at 5100 m falls along the LMWL and is the only meteoric water sample depleted in δD (more negative value) with respect to the thermal waters (Fig. 3).

Table 2Summary of field measurements and isotopic values at the different locations identified in Fig. 1.

Location	Type	N	$T_{mean} (^{\circ}C)$	$pH_{mean} \\$	C_{mean} (mS/cm)	$Cl^{a}\left(g/L\right)$	δO^{18}_{mean}	δD_{mean} (‰)	Q(L/s)	³ H (TU)
UB	Eruptive	11	84.6 ± 1.9	7.3 ± 0.4	14.6 ± 0.9	7.3 ± 0.4	-4.79 ± 0.46	-69.95 ± 1.91	-	_
	Non-eruptive	13	72.1 ± 11.0	6.8 ± 0.4	14.2 ± 2.3	7.1 ± 1.0	-4.59 ± 0.11	-70.25 ± 5.81	-	-
	Stream (#0)	1	36.3	7.8	7.4	3.0	-6.16	-58.30	250	0.14 ± 0.04
	Wetland (GW)	1	35.7	7.6	1.3	0.0	-9.08	-57.90	0.5	0.28 ± 0.03
VR	Eruptive (#225)	1	85.6	6.9	15.5	7.91	-4.61	-69.40		< 0.05
	Non-eruptive	9	70.3 ± 8.9	6.3 ± 0.5	7.8 ± 5.9	3.3 ± 2.2	-4.42 ± 2.38	-65.91 ± 6.38		-
	Mud pools	39	72.6 ± 12.1	_	_	-	_	-	-	-
MB	Eruptive	8	85.7 ± 1.0	7.2 ± 0.2	13.9 ± 0.9	6.9 ± 0.4	-5.24 ± 0.62	-67.60 ± 1.20	0.1 - 5.8	-
	Non-eruptive	1	74.7	7.0	15.2	7.7	-4.13	-65.70	-	-
	Stream North fork (#112)	1	23.8	7.3	13.9	6.9	-1.93	-53.40	15	< 0.05
	Stream South fork (#113)	1	21.2	7.9	12.1	5.9	-3.94	-61.40	3.8	< 0.05
SE	Non-eruptive	2	82.3 ± 1.2	7.4 ± 0.4	0.7 ± 0.0	0.0	-3.38 ± 1.75	-50.30 ± 1.84	-	-
	Mud pools	11	75.6 ± 9.3	-	_	-	-	-	-	-
	Stream (#100)	1	21.4	7.2	14.4	7.2	-0.07	-46.40	4.7	0.18 ± 0.05
TS	Eruptive	1	86.6	7.7	11.9	5.7	-6.04	-70.10	-	-
	Non-eruptive	1	68.4	7.4	10.0	4.6	-6.28	-70.20	-	-
	Tatio stream (#400)	1	38.9	8.3	3.8	0.7	-7.14	-57.80	140	< 0.05
LB	Eruptive	8	84.8 ± 2.0	7.3 ± 0.4	12.1 ± 0.4	5.8 ± 0.3	-5.88 ± 0.48	-70.50 ± 1.88	-	-
	Non-eruptive	8	77.2 ± 9.6	7.2 ± 0.3	12.0 ± 0.6	5.8 ± 0.4	-5.78 ± 0.31	-70.40 ± 1.28	-	-
	Stream Rio Salado (#1)	1	30.5	7.9	8.2	3.5	-5.72	-55.40	860	0.13 ± 0.05
SN	Snow	4	0.0	6.6 ± 0.6	0.0	0.0	-9.67 ± 1.06	-61.52 ± 9.84	-	-
Total num	Total number of measurements									

^a Cl estimated from the electrical conductivity.

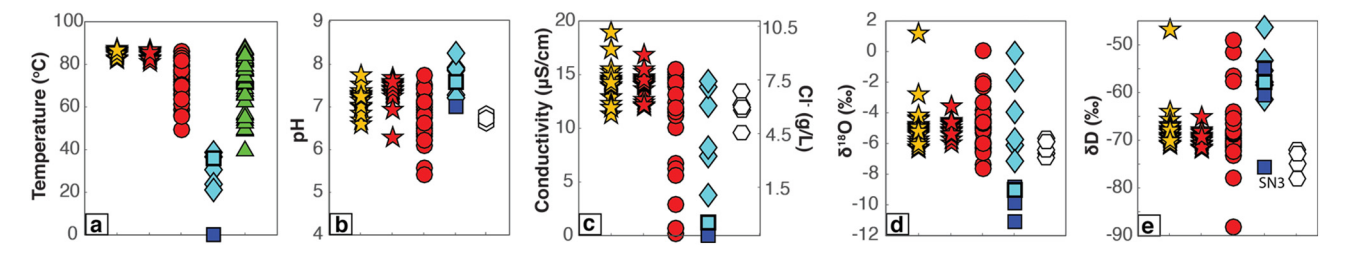


Fig. 2. Characterization of water samples according to the type of thermal feature. The symbols are the same as Fig. 1. (a) Temperature. We did not include the temperature of geothermal wells ($T_{max} > 200$ °C). (b) pH. (c) Electrical conductivity with scale on the left y-axis and Cl⁻ concentration on the right y-axis (derived from the electrical conductivity). (d) δ^{18} O. (e) δ D. Covariation of water characteristics is shown in Supplementary Figs. S1–S4.

Four samples have tritium concentrations above the analytical detection limit (>0.05 TU) (Table 2). Tritium in thermal water sample # 225 is below the detection limit, consistent with a previous study (Cortecci et al., 2005), indicating that most of the recharge occurred pre-1950. Sample GW has the highest ³H concentration (0.28 TU; Table 2), which is lower than concentrations previously reported for precipitation at El Tatio and adjacent areas in the Andes (Aravena et al., 1999; Cortecci et al., 2005; Houston, 2007; Boutt et al., 2016). Streams draining the thermal basins have ³H values lower than GW or below the detection limit, consistent with the dilution of thermal water with recent meteoric water.

Discharge and salinity measurements in the channels are summarized in Table 2 and Fig. 3. The highest discharge was measured in the channels upstream of the Salado River are in the UB, and the TS. Discharges in the channels of the MB were one order of magnitude lower than in the UB.

5. Discussion

Here, we discuss the new water chemistry, isotope and discharge data and how they address 1) the origin of water recharging the

reservoir, 2) the thermal state of the reservoir and 3) heat output from the system and how processes such as phase separation (Appendix A) and evaporation (Appendix B) affect the heat flow estimates.

5.1. Origin of the thermal waters

The concentrations of ³H measured in GW can be the result of mixing old meteoric water (pre-bomb) without ³H and small amounts of modern water with ³H. The absence of detectable tritium in thermal water indicates a residence time >60 years and lack of mixing with modern water. This new data contrasts with previous estimations of residence times of 10 to 17 years (Cusicanqui et al., 1975).

From geothermal well data (Giggenbach, 1978) and the isotopic composition of snow samples (Fig. 3), we infer that water in the deep reservoir has a meteoric origin with an isotopic composition similar to the composition of sample SN3 (-75.7% for δD and -11.07% for $\delta^{18}O$), which matches the theoretical values of groundwater of -78% for δD and -11% for $\delta^{18}O$, calculated by Cortecci et al., (2005). Assuming that the recharge of meteoric water occurs at elevations >5000 m, and thus about 15 km east of El Tatio, and considering the residence

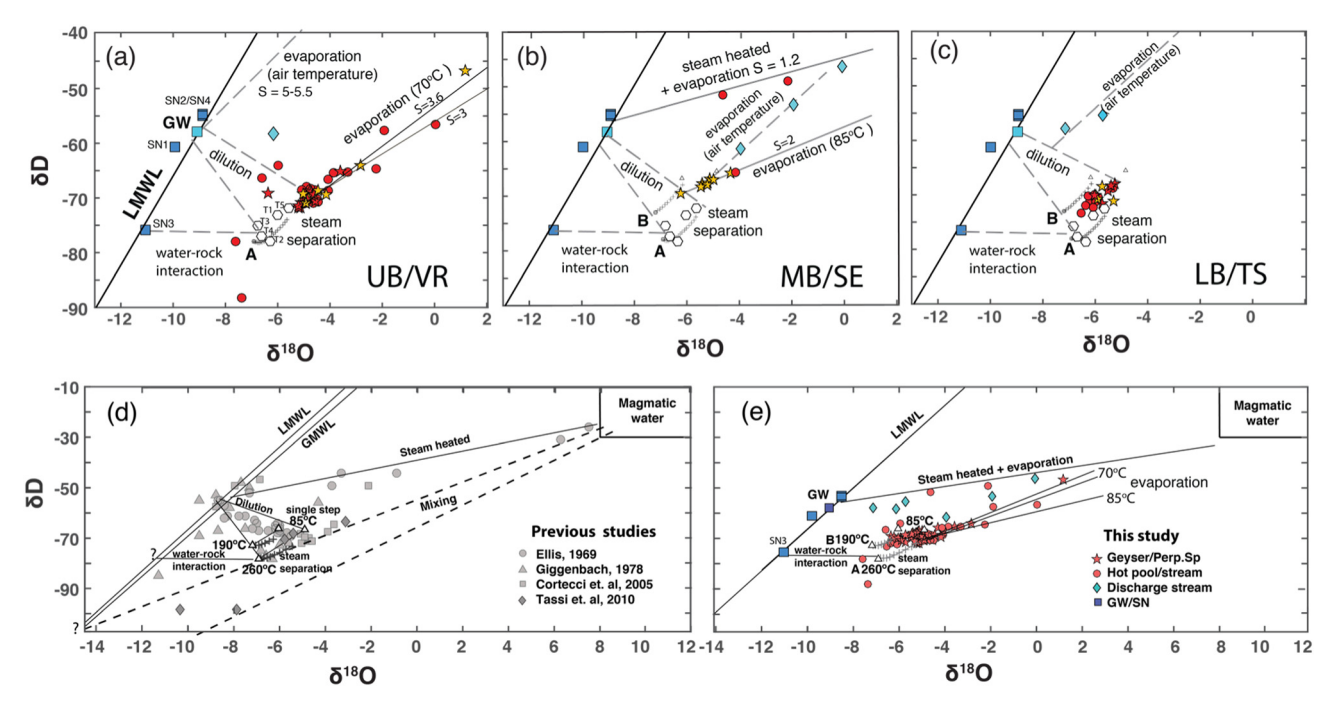


Fig. 3. Stable isotopes (δ^{18} O, δ D) and lines representing different processes shifting the composition from the local meteoric line (LMWL) δ^{18} O = 8.15 δ D + 15.3 defined for this area of the Andes (Aravena et al., 1999; Chaffaut et al., 1998). In this plot we used the same symbols as previous figures and added reservoirs A and B proposed by Giggenbach (1978). We computed the continuous steam separation from A and B starting at a temperature of 260 °C (reservoir A) and 190 °C (reservoir B) and decreasing in 20 °C steps until 80 °C (Appendix A). (a) Upper Basin (UB) compositions are more concentrated at the final step of the steam separation of A. Vega Rinconada (VR) compositions are spread along the dilution and evaporation lines (Appendix B). (b) For the Middle Basin (MB) the thermal features follow steam separation of B and evaporation (Appendix B). The South-east pools (SE) plot above the meteoric water line (LMWL) and follow the trend of steam-heated waters and evaporation described previously by Giggenbach (1978) (Appendix B). (c) Samples in the Lower Basin (LB) and the Tatio Stream (TS) are undistinguished, and they plot between the steam separations of both aquifers. (d) Summary of data and interpretation of the different processes affecting the fluids invoked in previous studies. (e) Data and interpretation from this study.

time assessed in this study, we estimate a time-averaged groundwater velocity of <0.25 km/year. This value is 4 to 5 times smaller than previous estimates (1 to 1.3 km/year; Cusicanqui et al., 1975; Muñoz and Hamza, 1993), likely resulting from differences in the estimation of residence times.

The isotopic shift of the reservoir water (geothermal wells) from the end members of meteoric water may be ascribed to water-rock interactions (horizontal lines in Fig. 3). Oxygen isotopic composition of Mesozoic to Quaternary igneous rocks in the central Andes have δ^{18} O between 6 and 11% (Longstaffe et al., 1983; Hamon et al., 1984). The observed shift requires exchange of a few tens of percent of oxygen. The major process affecting the ascending fluids from the reservoir is boiling and steam separation between the thermal reservoirs and the ground surface. Thermal waters appear to have isotopic compositions somewhat between the steam separation steps of the two reservoirs A and B defined by Giggenbach, 1978 (+ symbols shown in Fig. 3; Appendix A). Dilution with local meteoric water at depth is insignificant, in contrast to data reported in previous studies (Cusicangui et al., 1975; Giggenbach, 1978; Giggenbach and Stewart, 1982). The reason for the difference is not clear. A reduction in the meteoric water recharge in the last 40 years can explain this difference, though there is no statistically significant decrease in total precipitation (DGA, 2007, Heidinger et al., 2018).

Samples with enriched isotopic composition were found in previous studies, and these were explained by mixing with magmatic water (Cortecci et al., 2005; Tassi et al., 2010). However, that trend can be explained by increased evaporation, without the need to invoke exotic sources. More quantitatively, Fig. 3 and Supplementary Fig. S4 show how isotopic composition changes from evaporation at the surface. The slope of the evaporation line depends on the temperature of the thermal source (Appendix B). Considering the atmospheric conditions in the El Tatio high desert, evaporation may be the most important process affecting the isotopic composition of surface waters. The trends in the stable isotope data from thermal features can thus be explained by steam separation in the subsurface and evaporation at the surface, processes we know must occur, without requiring the addition of magmatic water.

5.2. Heat flow

Using the chemical composition of thermal water sample # 225 in Table 1 (VR geyser), we calculate reservoir temperatures by applying the SiO₂ and cation geothermometers (e.g., Fournier and Truesdell, 1973; Fournier, 1977, 1979; Giggenbach, 1988; Amorsson, 2000) and the iGeoT Multireaction Equilibrium Geothermometry (MEG) code (Spycher et al., 2013, 2014) (Table 3). For the iGeoT simulations, we assume that the dry gas is 100% CO₂, and consider a common assemblage of hydrothermal (secondary) minerals: calcite, quartz, albite, and smectite. Calculated results are presented in Table 3 and plotted Fig. 5a. The calculated SiO₂-Adiabatic temperature (196 °C) is considerably lower than the calculated Na-K temperatures (241 °C–254 °C) and the temperature calculated with iGeoT (230 \pm 11 °C) is intermediate. The

Table 3Calculated reservoir temperatures using different chemical geothermometers, the chemical composition of geyser sample # 225, and measured in the geothermal wells.

Geothermometer	T (°C)	Reference
SiO ₂ -adiabatic	196	Fournier (1977)
SiO ₂ -conductive	214	Fournier (1977)
Na-K-Ca	213	Fournier and Truesdell (1973)
Na-K	250	Fournier (1979)
Na-K	254	Giggenbach (1988)
Na-K	241	Amorsson (2000)
iGeoT	230 ± 11 °C	Spycher et al. (2013, 2014)
Well 1	211	Giggenbach (1978)
Well 7	260	Lahsen and Trujillo (1976)

lower reservoir temperatures inferred from the $\rm SiO_2$ geothermometer may be the result of polymerization and precipitation of silica, enhanced by the high salinity of the waters (e.g., Kley et al., 2017). The range of temperatures calculated is within the range of temperatures calculated by previous studies (e.g., Lahsen, 1976a,b; Giggenbach, 1978; Muñoz and Hamza, 1993; Cortecci et al., 2005; Tassi et al., 2005), and measured in the geothermal wells (Giggenbach, 1978; Lahsen and Trujillo, 1976). The calculated values are also similar to those calculated for geothermal reservoirs in other high-silica volcanic systems (e.g., King et al., 2016; Hurwitz and Manga, 2017).

We use the chloride inventory method to calculate the total discharge of thermal water into the Salado River by using the discharge and electrical conductivity of eruptive geysers in each basin or thermal group (Fig. 4). We assume zero background chloride (snowmelt). Starting upstream in the hydrological basin, we calculate that in the UB the discharge of thermal water varies between 85 L/s based on average measured Cl, and 92 L/s based on maximum Cl. For the SE and MB, the conductivity of each thermal group is higher than in the discharge channel, which implies some addition of meteoric water. For those two areas we consider the discharge in the channel to be the discharge of thermal water, which is equivalent to 20 L/s. For the TS, we calculated a thermal discharge of 38 L/s. The input of the LB group is 88 L/s for the average Cl to 92 L/s for the maximum Cl, considering the proportional contribution of every group upstream. As a result, the total amount of thermal discharge is between 218 and 234 L/s depending on the value of Cl concentration used for the calculation. Together, the UB and the LB contribute about 80% of the total thermal water into the Salado River.

The advective heat flow (W_T) assumes adiabatic decompression and cooling of liquid from a deep reservoir:

$$W_T = Q_T \rho C_p$$

with water discharge ($Q_T = 218$ to 234 L/s), water heat capacity ($C_p = 4.24$ kJ/kg °K) and a temperature difference (ΔT) between the reservoir ($T = 230 \pm 11$ °C; Table 3) and boiling at the ground surface (T = 86.6 °C), we estimate that the heat flow from the El Tatio geothermal system is between 121 and 141 MW. If we consider the highest temperature measured in the geothermal wells of 260 °C rather than the calculated reservoir temperature, then the calculated heat flow is slightly higher, 159 and 170 MW. We estimate the partitioning of heat flow between vapor and liquid assuming adiabatic decompression and cooling of the fluid from the reservoir to the surface. We estimate that 25 wt% of

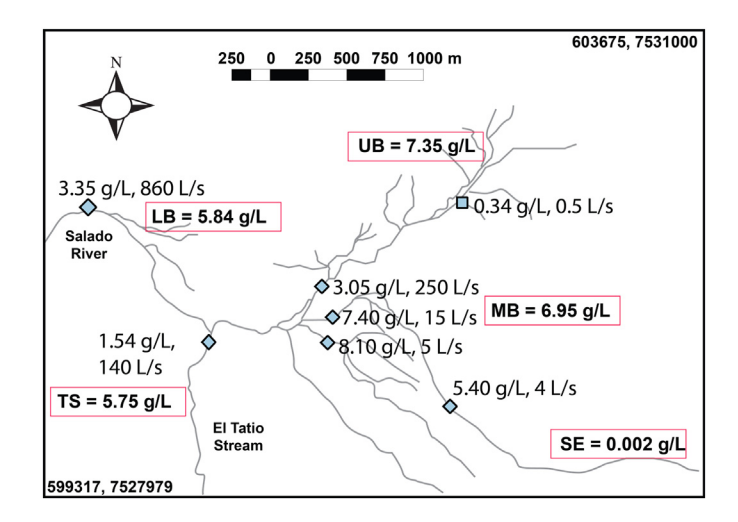


Fig. 4. Drainage system of the El Tatio basin. The points indicate the channels where discharge measurements were made (same symbols as Fig. 1). We added the measured values of chloride concentration and total discharge (Q value in Table 2). Values in red boxes present the mean chloride values of thermal water of each thermal basin.

steam is released by adiabatic decompression (Fig. 5b) carrying to the surface 113 MW. Additionally, the 75 wt% of liquid water transports 46 MW.

The reservoir was estimated to have a thickness between 150 m and 600 m (Lahsen and Trujillo, 1976; Aravena et al., 2016), and the thickness of the ignimbrite that hosts the reservoir was estimated to average 430 m (Lahsen and Trujillo, 1976). The minimum area constrained by wells is 11.5 km², and the maximum by geophysical surveys is 30 km² (Lahsen and Trujillo, 1976). Assuming a mean porosity of 10%, the volume of water in the reservoir is between 1.73 \times 10 11 and 1.95 \times 10 12 L. Dividing these volumes by the thermal discharge (minimum 218 L/s), the mean residence time in the reservoir estimated to be between 25 and 286 years.

The mean annual precipitation at El Tatio at 4370 m elevation over the last 40 years is 44 mm/year, with a maximum of 160 mm/year (DGA, 2007). Assuming that precipitation is the same everywhere, a recharge area of at least 155 km² is required to balance the minimum surface discharge of thermal water of 218 L/s. This value assumes total infiltration of rainwater into the deep reservoir and no surface runoff or evapotranspiration at the surface and hence is a lower bound for the recharge area.

We find that the discharge of thermal water calculated from October 2014 measurements agrees with the data collected in the dry seasons during the 1970s (Trujillo, 1974). For comparison, the thermal discharge from El Tatio is an order of magnitude less than the thermal discharge from Yellowstone, USA (3200 L/s, Fournier, 1989) and the Domuyo Volcano in Patagonia of about 1 GW (Chiodini et al., 2014), but more than that of the Mutnovsky geothermal field in Kamchatka, Russia (80 L/s before drilling, Vakin and Pilipenko, 1986), Wairakei, New Zealand before exploitation (100 L/s, Ellis and Wilson, 1955) and Lassen Peak, USA (20 L/s, Sorey, 1986). Comparable values of advective heat flow were calculated for Wairakei of 188 MW (Glover and Mroczek, 2009) and El Chichon in Mexico of 175 MW (Taran and Peiffer, 2009).

To provide a quantitative context for the calculated heat output from the entire El Tatio basin using the chloride inventory method, we quantified heat output from the vigorous, El Jefe (EJ) geyser (an unofficial name; Munoz-Saez et al., 2015a,b) which had periodic eruptions every 110 s during our study in 2014. To quantify heat output from the geyser, we added 125 L of ~15 °C water to the conduit during one quiescent period, similar to the type of experiment performed by Shteinberg et al. (2013). Before, during, and after the experiment, we recorded the eruptions with a video camera, and we recorded pressure (accuracy of 2.5%) and temperature (1 °C accuracy) at a depth of 1.5 m in the conduit every 1 s. After the addition of cold water (Fig. 6), the temperature in the

conduit decreased from 86 °C to 69 °C in <30 s and water level in the conduit rose by 0.8 m (7 kPa) and reached the ground surface. Immediately following the addition of water, the geyser skipped two eruptions. Despite the lack of erupted water, the periodic signals of pressure and temperature that accompany normal eruptions continued. The geyser resumed the 110 s eruptive cycle after the two missed eruptions and water in the conduit was heated to the boiling temperature.

We calculate that $\sim 3.4 \times 10^4$ kJ were needed to warm the 125 L of added water from 15 °C to 86.6 °C (using $H_{\text{erupted}} = C_p m \Delta T$, and $C_p =$ 4.2 kJ/kg °K). This occurs over two eruption cycles, which results in 0.14 MW per cycle (eruption time 120 s). Previous studies at El Jefe geyser showed that the temperature increase before an eruption is 3 °C and the mass of erupted water is 110 kg (Munoz-Saez et al., 2015a). From these data, Munoz-Saez et al. (2015a) estimated that the heat required for one eruption was one order of magnitude lower $\sim 1.6 \times 10^3$ kJ, corresponding to an average heat flow of 0.013 MW; the lower value is the result of neglecting heat transport by vapor. The heat flow estimated from the experiment at El Jefe gevser (0.14 MW) is only a very small fraction (~0.1%) of the minimum calculated heat output from El Tatio (121 MW). The present data suggests that about 90% of the heat added to the conduit is discharged as latent heat in vapor. A similar inference was made on the heat output from the more voluminous Lone Star geyser, which is only a very small fraction of the total heat output from the Yellowstone Plateau Volcanic Field (Karlstrom et al., 2013).

We summarize our conceptual model in Fig. 7. Snowmelt from the mountains at elevations >5000 m to the east of El Tatio is recharged through fractures and faults in the volcanic units. Water is heated in two deep reservoirs at different depths and interacts with the surrounding rock for >60 years before ascending adiabatically and boiling in the subsurface. Presumably the boiling happens at the shallowest depths to ascending reservoir fluids prior to and during eruptions. Residual liquid mixes with, and heats, to varying degrees local meteoric water (<5000 m) in the shallow subsurface. In marshes in VR and SE, mixing of meteoric with thermal water and steam heating of shallow water occurs as the water table reaches the surface. At the ground surface, thermal water evaporates to different degrees. Geysers lose steam to the atmosphere as they erupt. The geochemical, temperature and discharge measurements compiled in the present study quantify the extent of steam separation, mixing and evaporation and allow us to quantify the total discharge of thermal fluids and heat.

There remain open questions about the recharge and heat budgets. What are the recharge rates? We only obtained an upper bound for the infiltration rate of the water recharging the system. How does the

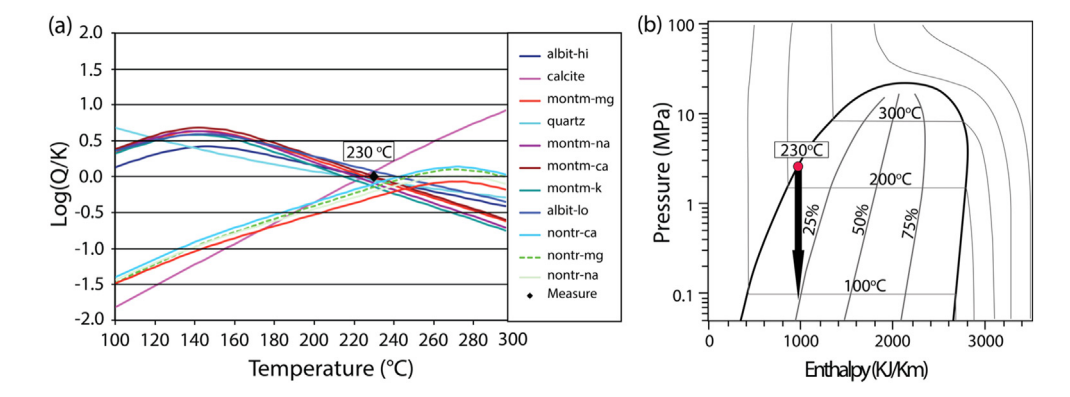


Fig. 5. (a) Reservoir temperature calculated with the iGeoT Multireaction Equilibrium Geothermometry (MEG) code (Spycher et al., 2013, 2014). We calculated the saturation indices log (Q/K) of the minerals as a function of temperature. The mineral assemblage used for the calculation is described in the legend. The lines cross near zero, close to an average temperature of 230 ± 11 °C. This temperature is the inferred reservoir temperature. (b) Diagram of pressure-enthalpy for pure water showing two-phase region (bounded by thick solid line). Inside of that region, the contours of equal temperature are the horizontal lines and the mass fractions of steam are the vertical lines. The red circle denotes the conditions of the reservoir fluid: at 230 °C the enthalpy of steam is 2603 kJ/kg, and the arrow represents adiabatic decompression to the ground surface where the average temperature is 86.6 °C. In that process, 25 wt% steam is released.

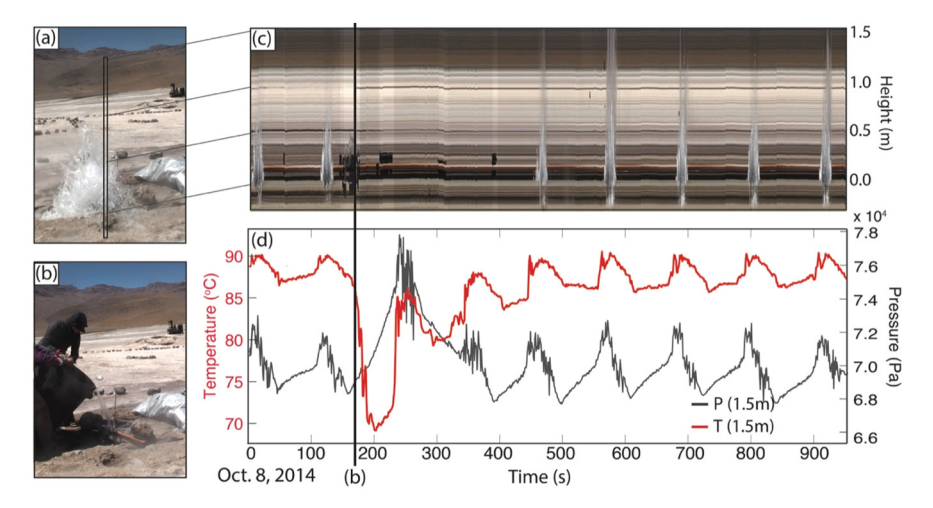


Fig. 6. Experiment at El Jefe geyser (informal name; Munoz-Saez et al., 2015a,b). (a) Photo of the geyser erupting at the surface (time = 10 s after eruption onset). (b) Photo of cold water being added to the geyser conduit (time = 170 s after eruption onset). (c) Stacked video images showing time series of an eruption on Oct. 8, 2014, starting at 15:45:52 UTC; height 0.0 corresponds to the base of the geyser shown in the rectangle in panel (a). (d) Time series of pressure (*P*) and temperature (*T*) recorded by sensors inside the conduit, 1.5 m below the ground surface.

discharge of thermal water vary over timescales of decades to thousands of years? How old is the El Tatio geothermal system? Where is the heat source? By monitoring the thermal manifestations and cold streams we can obtain the environmental baseline of the geothermal system. A combination of this information with geophysical surveys and detailed structural geology can provide a better understanding of connections between deep aquifers, shallow aquifers and the heat sources. Studying the hydrothermal deposits may also provide insights into the development and evolution of the geothermal system on time scales of hundreds to thousands of years.

6. Conclusions

This study provides data that confirm some of the ideas proposed from the 1970s and adds new information about the El Tatio geothermal system:

Hydrogen and oxygen isotopes indicate that the source of the recharge water is snowmelt at elevations >5000 m >15 km east of El Tatio, and that over time this water interacts with the surrounding rock to generate the fluids in the geothermal reservoir.

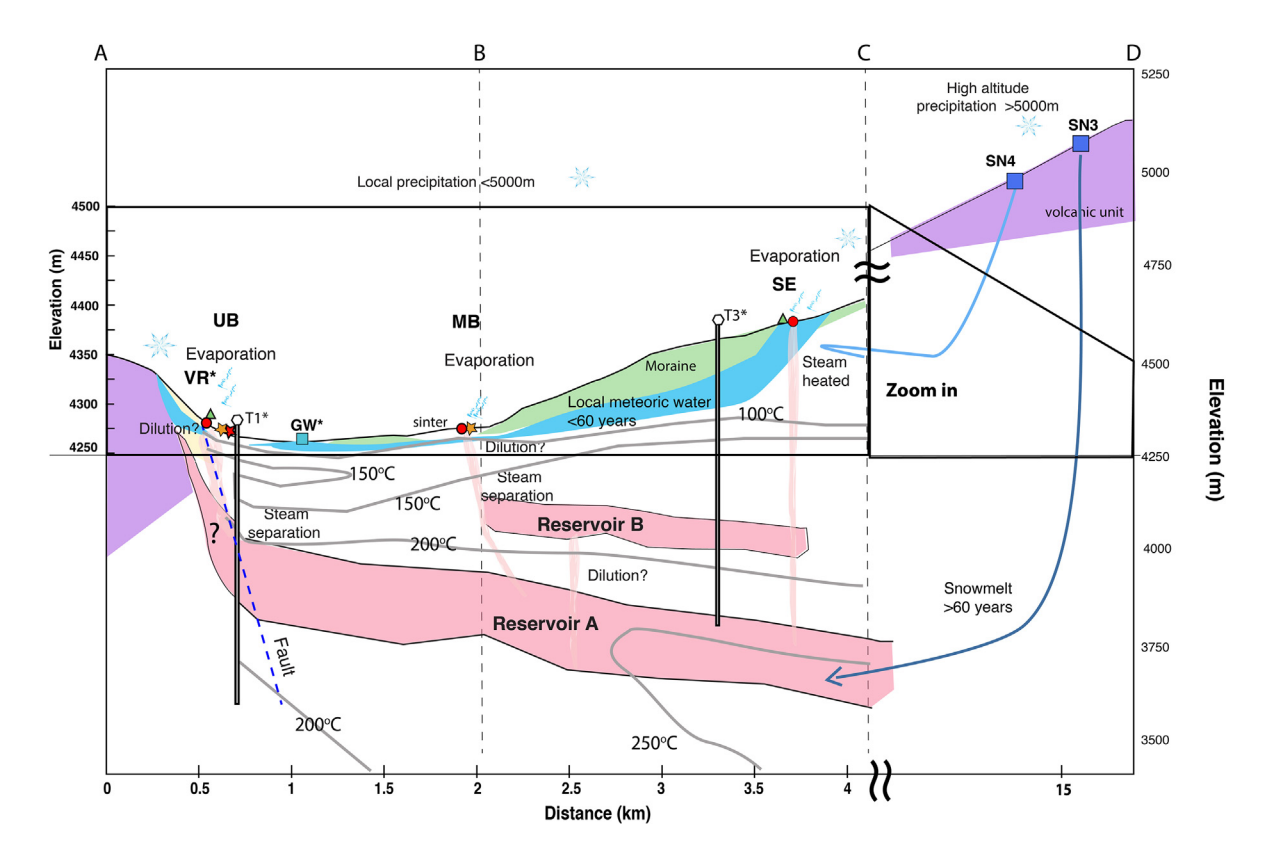


Fig. 7. Vertical cross-section showing a conceptual model of the El Tatio geothermal field summarizing the main processes affecting the composition of the thermal fluids. Profile is defined in Fig. 1. The elevation is exaggerated by a factor of 4 on the left y-axis and a factor of 2 on the right y-axis. The x-axis is not continuous. Well temperatures were extracted from Healy and Hochstein (1973), where the main deeper aquifer A was described as a fractured ignimbrite called Puripicar. The temperature and depth of reservoir B was extracted from Lahsen and Trujillo (1976).

- From tritium data and assuming a meteoric origin, we infer that local ground water has a time-averaged residence time of <60 years, while thermal water has >60 years residence time.
- The main process affecting the ascending fluids is steam separation from deep reservoirs. Dilution of the thermal reservoir fluids with local meteoric water at different depths is insignificant, but evaporation from pools is significant.
- The calculated advective heat discharge from El Tatio is between 120 and 170 MW, similar to values estimated at Wairakei in New Zealand and El Chichon in Mexico.
- Total discharge of thermal water at El Tatio in October 2014 was 218 to 234 L/s and is similar to previous estimates, suggesting little change over the past 40 years.

These findings provide land managers and policymakers data to inform sustainable management of potential geothermal development in the area, while at the same time protecting the unique thermal features in this natural system.

Acknowledgments

This study was supported by the National Science Foundation (EAR1724986), CEGA-University of Chile, Conicyt (Postdoctoral fellowship ID 3170007), Center for Latin American Studies-University of California Berkeley, and the Judy Webb Chair. We thank those who provided essential help in the field: Angello Negri, Camilo Gonzalez, Alberto Ardid, Prof. Atsuko Namiki, Prof. Martin Reich and Prof. Emilio Vera. We thank Mark Huebner, Bill Evans and Deb Bergfeld for chemical analyses at the U.S. Geological Survey laboratories in Menlo Park, California and Andy Hunt at the U.S. Geological Survey Noble Gas Laboratory in Denver, Colorado for the tritium analysis. We thank Felipe Aguilera for the digital version for the geological map of El Tatio. The fieldwork was performed with the permission of the Amayras Communities of Caspana and Toconce. We thank Deb Bergfeld, Franco Tassi, anonymous reviewer and editors Alessandro Aiuppa and Michael Clynne for their constructive comments and suggestions. Any use of trade, firm, or product names is for descriptive purposes and does not imply endorsment by the U.S. Government.

Appendix A. Steam separation

Steam separation may occur in a single stage or as part of a continuous process (e.g., Truesdell et al., 1977; Giggenbach, 1978; Giggenbach and Stewart, 1982): (1) during single step separation the steam and water are contact and maintain isotopic equilibrium until the steam separates at the surface; (2) during continuous steam separation the steam is removed continuously as soon as it is formed. In natural systems the separation of steam occurs in between these two end members. During both these processes, as steam is removed, the remaining liquid is enriched in the heavier isotopes.

In a single stage steam separation, water at some initial temperature (T_i) boils adiabatically, and steam and liquid separate at temperature (T_f) . The mass fraction of the remaining liquid after boiling (f_{steam}) is obtained from the enthalpy (H):

$$f_{steam} = \frac{\left(H_{liq(i)} - H_{liq(f)}\right)}{\left(H_{steam(f)} - H_{liq(f)}\right)},\tag{A1}$$

where $H_{liq(i)}$ is the enthalpy of the initial non-separated liquid, and $H_{liq(f)}$ and $H_{steam(f)}$ the enthalpy of the final liquid and steam, respectively.

Assuming that isotopic fractionation during a phase change is an equilibrium process governed by a constant fractionation factor (α) , and approximately proportional to isotopic concentration of the liquid

 (δ_{liq}) and steam (δ_{steam}) at a given temperature (e.g. Truesdell et al., 1977; Giggenbach and Stewart, 1982)

$$\delta_{lig} - \delta_{steam} \approx 1000 \ln(\alpha)$$
 (A2)

we can evaluate the isotopic composition of residual liquid after steam separation as a function of the residual mass fraction (Giggenbach and Stewart, 1982):

$$\delta_{\textit{liq}(f)} = \delta_{\textit{liq}(i)} + (f_{\textit{steam}} * 1000 \, \ln(\alpha)) \tag{A3}$$

Similarly, for continuous step steam separation, the concentrations of both isotopes can be calculated at every step.

We analyzed waters from the different areas of the El Tatio geothermal field, and we calculated the steam separation line for single step and continuous steam separation. We evaluated the values for fractionation factors (α) at different temperatures from data available in the literature (Majoube, 1971; Horita and Wesolowski, 1994; Horita et al., 1995).

Two reservoirs had been proposed based on measurements from geothermal wells (e.g., Cusicanqui et al., 1975; Giggenbach, 1978; Cortecci et al., 2005): a hot reservoir (A) of 260 °C to 270 °C, $\delta^{18} O_A \sim -6.9\%$, and $\delta D_A \sim -78\%$, that feeds the UB and VR, and a colder and more diluted reservoir (B) of 170 °C to 190 °C, $\delta^{18} O_B \sim -7.2\%$ and $\delta D_B \sim -73\%$ that supplies water to the MB and LB (e.g., Cusicanqui et al., 1975; Giggenbach, 1978).

Appendix B. Evaporation and dilution

Given the dry and windy environment at El Tatio, evaporation may play an important role in the isotopic fractionation of water sources that are constantly exposed to the atmosphere. Pools with a large surface area exposed to the atmosphere or frequent eruptions would be subjected to high evaporation rates. This effect has been documented before only in the southeast side of our main study area (Giggenbach, 1978; Giggenbach and Stewart, 1982). In the rest of the geyser field, the greater effect of dilution probably masked the effects of evaporation.

We assume that evaporation responds only to the kinetic fractionation and that it is given by the simplified Rayleigh distillation equation

$$\delta_{liq} - \delta_e = \epsilon_k \tag{B1}$$

where δ_{liq} is the isotopic composition of liquid, δ_e is the composition of the evaporated vapor, and ϵ_k is the kinetic fractionation factor. The kinetic fractionation factor and the slope defined by kinetic fractionation of deuterium and oxygen ($\epsilon_{kD}/\epsilon_{k180}$) depend on the temperature of the water (Craig, 1961, 1963; Welhan and Fritz, 1977).

At 70 °C, close to the average temperature of thermal pools in the UB and VR (Table 2), the kinetic values are $\varepsilon_{kD}=50$ and $\varepsilon_{k180}=16$ and the slope defined by kinetic fractionation $\varepsilon_{kD}/\varepsilon_{k180}$ is 3.1 (Craig, 1963; Welhan and Fritz, 1977; Horita et al., 2008). This slope is similar to the slope S = 3.6 ($\rm r^2=0.96$) defined by the linear fit of the isotopic values for all hot springs that are enriched in δ^{18} O and δD after steam separation from A (Fig. 3). Even closer is the fit to the slope S = 3 ($\rm r^2=0.92$) defined by the linear fit to data from non-eruptive thermal pools in the area.

In the MB, the isotopic values of thermal features deviate further from steam separation from reservoir B (Fig. 3b). The linear regression of the isotopic values generates a line of slope S = 2 ($r^2 = 0.97$). This slope is similar to slope defined by kinetic fractionation at the boiling temperature of ~85 °C with values of $\varepsilon_{kD} = 42.4$, $\varepsilon_{k180} = 15.7$, and $\varepsilon_{kD}/\varepsilon_{k180} = 2.6$ (e.g., Craig et al., 1963; Welhan and Fritz, 1977; Horita et al., 2008). Thermal features in the MB are large pools of >2 m diameter with permanent fountain eruptions. These results are consistent with features that are constantly erupting at the boiling temperature.

Further southeast of our study area, the isotopic composition of waters was attributed to steady state evaporation of local meteoric water that had been heated by steam from the hot reservoir A (Giggenbach, 1978; Giggenbach and Stewart, 1982; Cortecci et al., 2005). The slope of steam-heated waters (S_{SH}) was estimated as (Giggenbach and Stewart, 1982)

$$S_{SH} = \frac{(\delta D_A - \delta D_{GW} + \epsilon_{kD})}{\left(\delta^{18} O_A - \delta^{18} O_{GW} + \epsilon_{k180}\right)} = 1.2 \tag{B2}$$

where δD_A and $\delta^{18}O_A$ correspond to the deuterium and oxygen isotopic composition of the main reservoir A. Data from previous studies found slopes between 1.6 and 2 (Giggenbach, 1978; Giggenbach and Stewart, 1982; Cortecci et al., 2005). Evaluating our data from the low-chloride waters in the SE, the line generated from the isotopic data and GW give a slope of ~1.3 ($r^2 = 0.99$).

Even though these models are simplified, and the slope for the isotope ratios will strongly depend on the temperature of evaporation, they seem to capture the main processes affecting the isotopic composition of thermal waters. Additional processes can be included. For example, the evaporation effect calculated from the Rayleigh distillation equation neglects the relative humidity of the atmosphere, the isotopic composition of the atmosphere and the effect of the wind.

In LB and TS, dilution of thermal waters along the Salado River plays a more important role (Fig. 3c). The evaporation effects are less clear due to the contributions from fresh water in the river. Low chloride thermal pools in VR show that <30% of local meteoric water dilutes the thermal reservoir water (Fig. 3a). The dilution might occur at shallow depths given that VR is a marsh. Continuous dilution at different depths was previously identified as one of the most important process affecting thermal features (Giggenbach, 1978; Giggenbach and Stewart, 1982) for samples collected at the end of the 1960s and beginning of the 1970s (e.g. Ellis, 1969; Cusicanqui et al., 1975; Giggenbach, 1978; Giggenbach and Stewart, 1982). However, our samples collected in 2014 show <10% dilution for the MB and LB, and shallow dilution of <30% in VR, and that continuous dilution at different depths is insignificant. This difference may arise because samples were collected during different seasons, or local meteoric recharge decreased over time.

Shallow waters may also be affected by the addition of deeper gases. We observed bubbling mud pools with temperatures below the boiling point, suggesting that CO_2 is being delivered from below. Some pools in the UB, and especially in VR, show moderate-acid pH that tends to decrease with decreasing temperature. pH may be reduced by addition of CO_2 . The chemistry of the pool in VR showed high HCO_3^- compared with CI^- and SO_4^{2-} (Table 1, sample # 231), which occurs through conversion of dissolved CO_2 to HCO_3^- , typical of peripheral waters located at the margins of major up-flow zones (e.g., Giggenbach and Soto, 1992; Giggenbach et al., 1994). However, we have the chemistry of only one sample.

Appendix C. Supplementary data

Supplementary data to this article can be found online at https://doi.org/10.1016/j.jvolgeores.2018.07.007.

References

- Amorsson, S., 2000. The quartz-and Na/K geothermometers. I. New thermodynamic calibration. Proceedings of the World Geothermal Congress, pp. 929–934.
- Aravena, R., Suzuki, O., Pena, H., Pollastri, A., Fuenzalida, H., Grilli, A., 1999. Isotopic composition and origin of the precipitation in Northern Chile. Appl. Geochem. 14 (4), 411–422.
- Aravena, D., Muñoz, M., Morata, D., Lahsen, A., Parada, M.Á., Dobson, P., 2016. Assessment of high enthalpy geothermal resources and promising areas of Chile. Geothermics 59, 1–13.
- Bayer, R., Schlosser, P., Bonisch, G., Rupp, H., Zaucker, F., Zimmek, G., 1989. Performance and blank components of a mass spectrometic system routine measurement of

- helium isotopes and tritium by 3He ingrowth method. Sitzungsber. Heidelb. Akad. Wiss. Math. Naturwiss. Kl. 89. https://doi.org/10.1007/978-3-642-48373-8 (44 pp.).
- Boutt, D.F., Hynek, S.A., Munk, L.A., Corenthal, L.G., 2016. Rapid recharge of fresh water to the halite-hosted brine aquifer of Salar de Atacama, Chile. Hydrol. Process. 30 (25), 4720–4740.
- Chaffaut, I., Coudrain-Ribstein, A., Michelot, J.L., Pouyaud, B., 1998. Prècipitations d'altitude du Nord-Chile, origine des sources de vapeur et données isotopiques. Bull. Inst. Fr. Études Andines 27, 367–384.
- Chiodini, G., Liccioli, C., Vaselli, O., Calabrese, S., Tassi, F., Caliro, S., ... D'alessandro, W., 2014. The Domuyo volcanic system: an enormous geothermal resource in Argentine Patagonia. J. Volcanol. Geotherm. Res. 274, 71–77.
- Coleman, M.L., Shepherd, T.J., Durham, J.J., Rouse, J.E., Moore, G.R., 1982. Reduction of water with zinc for hydrogen isotope analysis. Anal. Chem. 54 (6), 993–995.
- Corbett, D.M., 1943. Stream-gaging Procedure, A Manual Describing Methods and Practices of the Geological Survey (No. 888). US Govt. Print. Off.
- Cortecci, G., Boschetti, T., Mussi, M., Lameli, C.H., Mucchino, C., Barbieri, M., 2005. New chemical and original isotopic data on waters from El Tatio geothermal field, northern Chile. Geochem. J. 39 (6), 547–571.
- Craig, H., 1961. Isotopic variations in meteoric waters. Science 133, 1702-1703.
- Craig, H., 1963. The isotopic geochemistry of water and carbon in geothermal areas. Nuclear Geology on Geothermal Areas, pp. 17–53.
- Craig, H., Gordon, L.I., Horibe, Y., 1963. Isotopic exchange effects in the evaporation of water: 1. Low-temperature experimental results. J. Geophys. Res. 68 (17), 5079–5087.
- Cusicanqui, H., Mahon, W.A.J., Ellis, A.J., 1975. The geochemistry of the El Tatio geothermal field, Northern Chile. Second United Nations Symposium on the Development and Utilization of Geothermal Resources, San Francisco, pp. 703–711.
- DGA Direccion general de aguas de chile, 2007. Información Oficial Hidrometeorológica y de Calidad de Aguas en Línea. http://snia.dga.cl/BNAConsultas/reportes, Accessed date: March 2017.
- Ellis, A.J., 1969. Survey for geothermal development in Northern Chile. Preliminary Geochemistry Report, El Tatio Geothermal Field. UNDP-Report.
- Ellis, A.J., Wilson, S.H., 1955. The heat from the Wairakei-Taupo thermal region calculated from the chloride output. N. Z. J. Sci. Technol. B Gen. Res. Sect. 36, 622–631.
- Epstein, S., Mayeda, T., 1953. Variation of O18 content of waters from natural sources. Geochim. Cosmochim. Acta 4 (5), 213–224.
- Fournier, R.O., 1977. Chemical geothermometers and mixing models for geothermal systems. Geothermics 5 (1–4), 41–50.
- Fournier, R.O., 1979. A revised equation for the Na/K geothermometer. Geotherm. Resour. Counc. Trans. 3, 221–224.
- Fournier, R.O., 1989. Lectures on Geochemical Interpretation of Hydrothermal Waters (No. 10). UNU Geothermal Training Programme.
- Fournier, R.O., Truesdell, A.H., 1973. An empirical Na/K/Ca geothermometer for natural waters. Geochim. Cosmochim. Acta 37 (5), 1255–1275.
- Giggenbach, W.F., 1978. The isotopic composition of waters from the El Tatio geothermal field, Northern Chile. Geochim. Cosmochim. Acta 42, 979–988.
- Giggenbach, W.F., 1988. Geothermal solute equilibria. Derivation of Na-K-Mg-Ca geoindicators. Geochim. Cosmochim. Acta 52 (12), 2749–2765.
- Giggenbach, W.F., Soto, R.C., 1992. Isotopic and chemical composition of water and steam discharges from volcanic-magmatic-hydrothermal systems of the Guanacaste Geothermal Province, Costa Rica. Appl. Geochem. 7 (4), 309–332.
- Giggenbach, W.F., Stewart, M.K., 1982. Processes controlling the isotopic composition of steam and water discharges from steam vents and steam-heated pools in geothermal areas. Geothermics 11 (2), 71–80.
- Giggenbach, W.F., Sheppard, D.S., Robinson, B.W., Stewart, M.K., Lyon, G.L., 1994. Geochemical structure and position of the Waiotapu geothermal field, New Zealand. Geothermics 23 (5-6), 599–644.
- Glennon, J.A., Pfaff, R.M., 2003. The extraordinary thermal activity of El Tatio Geyser Field, Antofagasta Region, Chile. GOSA Trans. 8, 31–78.
- Glover, R.B., Mroczek, E.K., 2009. Chemical changes in natural features and well discharges in response to production at Wairakei, New Zealand. Geothermics 38, 117–133.
- Hamon, R.S., Barreiro, B.A., Moorbath, S., Hoefs, J., Francis, P.W., Thorpe, R.S., Deruelle, B., McHugh, J., Viglino, J.A., 1984. Regional O-, Sr- and Pb-isotope relationships in late Cenozoic calc-alkaline lavas of the Andean Cordillera. J. Geol. Soc. Lond. 141, 202, 222
- Healy, J., Hochstein, M.P., 1973. Horizontal flow in hydrothermal systems. J. Hydrol. N. Z. 71–82.
- Heidinger, H., Carvalho, L., Jones, C., Posadas, A., Quiroz, R., 2018. A new assessment in total and extreme rainfall trends over central and southern Peruvian Andes during 1965–2010. Int. J. Climatol. 38, 998–1015.
- Hochstein, M.P., 1971. Geophysical survey of the El Tatio Geothermal area, results up to December 1970. UN Project Report.
- Horita, J., Wesolowski, D.J., 1994. Liquid-vapor fractionation of oxygen and hydrogen isotopes of water from the freezing to the critical temperature. Geochim. Cosmochim. Acta 58 (16), 3425–3437.
- Horita, J., Cole, D.R., Wesolowski, D.J., 1995. The activity-composition relationship of oxygen and hydrogen isotopes in aqueous salt solutions: III. Vapor-liquid water equilibration of NaCl solutions to 350 C. Geochim. Cosmochim. Acta 59 (6), 1139–1151.
- Horita, J., Rozanski, K., Cohen, S., 2008. Isotope effects in the evaporation of water: a status report of the Craig-Gordon model. Isot. Environ. Health Stud. 44 (1), 23–49.
- Houston, J., 2007. Recharge to groundwater in the Turi Basin, northern Chile: an evaluation based on tritium and chloride mass balance techniques. J. Hydrol. 334 (3), 534–544.
- Hurwitz, S., Manga, M., 2017. The fascinating and complex dynamics of geyser eruptions. Annu. Rev. Earth Planet. Sci. 45. 31–59.

- Hurwitz, S., Harris, R.N., Werner, C.A., Murphy, F., 2012. Heat flow in vapor dominated areas of the Yellowstone Plateau Volcanic Field: implications for the thermal budget of the Yellowstone Caldera. J. Geophys. Res. Solid Earth 117 (B10).
- Ingebritsen, S.E., Sherrod, D.R., Mariner, R.H., 1989. Heat flow and hydrothermal circulation in Cascade range, north-central Oregon. Science 243, 1458–1462.
- Ingebritsen, S.E., Galloway, D.L., Colvard, E.M., Sorey, M.L., Mariner, R.H., 2001. Time-variation of hydrothermal discharge at selected sites in the western United States: implications for monitoring. J. Volcanol. Geotherm. Res. 111 (1), 1–23.
- Karlstrom, L., Hurwitz, S., Sohn, R.A., Vandemeulebrouck, J., Murphy, F., Rudolph, M.L., Johnston, M.J.S., Manga, M., McCleskey, R.B., 2013. Eruptions at Lone Star Geyser, Yellowstone National Park, USA, part 1: energetics and eruption dynamics. J. Geophys. Res. Solid Earth 118, 1–15. https://doi.org/10.1002/jgrb.50251.
- King, J.M., Hurwitz, S., Lowenstern, J.B., Nordstrom, D.K., McCleskey, R.B., 2016. Multireaction equilibrium geothermometry: a sensitivity analysis using data from the Lower Geyser Basin, Yellowstone National Park, USA. J. Volcanol. Geotherm. Res 328 105–114
- Kley, M., Kempter, A., Boyko, V., Huber, K., 2017. Silica polymerization from supersaturated dilute aqueous solutions in the presence of alkaline earth salts. Langmuir 33 (24), 6071–6083.
- Lahsen, A., 1976a. La actividad geotermal y sus relaciones con la tectónica y el volcanismo en el norte de Chile. I Congreso Geológico Chileno, Actas, Antofagasta, pp. B105–B127.
- Lahsen, A., 1976b. Geothermal exploration in Northern Chile-Summary. Circum Pacific Energy and Mineral Resour. Conf., Honolulu, pp. 169–175.
- Lahsen, A., Trujillo, P., 1975. El Tatio geothermal field. Proc. of the Second United Nations Symposium on the Development and Use of Geothermal Resources, San Francisco, California, pp. 157–178.
- Lahsen, A., Trujillo, P., 1976. El campo geotermico de El Tatio, Chile. Proyecto Geotermico CORFO-ONU. Internal Report.
- Longstaffe, F.J., Clark, A.H., McNutt, R.H., Zentilli, M., 1983. Oxygen isotopic compositions of Central Andean plutonic and volcanic rocks, latitudes 26–29° south. Earth Planet. Sci. Lett. 64 (1), 9–18.
- Lucas, L.L., Unterweger, M.P., 2000. Comprehensive review and critical evaluation of the half-life of Tritium. J. Res. Nat. Inst. Stand. Technol. 105 (4), 541–550.
- Mahon, W.A.J., 1970. A geochemical assessment of the El Tatio geothermal field with particular reference to the fluids discharged from Holes, 1, 2, 3, and 4. UN Project Report.
 Mahon, W.A.J., 1972. Geochemical survey of the El Tatio geothermal area, summary of results, January, February, 1972. UN Project Report.
- Mahon, W.A.J., 1974. The geochemistry of El Tatio geothermal system. Survey for geothermal development in Chile. UN Project Report.
- Majoube, M., 1971. Oxygen-18 and deuterium fractionation between water and steam (in French). J. Chim. Phys. Phys.-Chim. Biol. 68, 1423–1436.
- Marinovic, N., Lahsen, A., 1984. Hoja Calama: región de Antofagasta: carta geológica de Chile 1: 250.000. Servicio Nacional de Geología y Minería, Chile.
- Muñoz, M., Hamza, V., 1993. Heat flow and temperature gradients in Chile. Stud. Geophys. Geod. 37 (3), 315–348.
- Munoz-Saez, C., Manga, M., Hurwitz, S., Rudolph, M., Namiki, A., Wang, C.-Y., 2015a. Dynamics within geyser conduits, and sensitivity to environmental perturbations: insights from periodic geyser in the El Tatio geyser field, Atacama Desert,

- Chile. J. Volcanol. Geotherm. Res. 292, 41–55. https://doi.org/10.1016/j.jvolgeores.2015.01.002.
- Munoz-Saez, C., Namiki, A., Manga, M., 2015b. Geyser eruption intervals and interactions: examples from El Tatio, Atacama, Chile. J. Geophys. Res. 120. https://doi.org/10.1002/ 2015JB012364.
- Navarro, 1972. Reconocimiento hidrogeologico de El Tatio, Provincia de Antofagasta. Estudio para el desarrollo geotermico en el norte de Chile. Biblioteca Servicio Nacional de Geologia y Mineria, Chile.
- Shteinberg, A., Manga, M., Korolev, E., 2013. Measuring pressure in the source region for geysers, Geyser Valley, Kamchatka. J. Volcanol. Geotherm. Res. 264, 12–16.
- Sorey, M.L., 1986. Hot Spring Monitoring at Lassen Volcanic National Park, California 1983–1985. Sponsored by the Geothermal and Hydropower Technologies Division of the US Department of Energy, Stanford-DOE Contract No. DE-AS03-80SF11459 and Contract No. DE-AS07-841D12529.
- Sorey, M.L., Lewis, R.E., 1976. Convective heat flow from hot springs in the Long Valley caldera, Mono County, California. J. Geophys. Res. 81 (5), 785–791.
- Spycher, N., Peiffer, L., Sonnenthal, E., 2013. GeoT users guide: a computer program for multicomponent geothermometry and geochemical speciation version 1.4. Lawrence Berkeley National Laboratory, Report No. LBNL-6172E.
- Spycher, N., Peiffer, L., Saldi, G., Sonnenthal, E., Reed, M.H., Kennedy, B.M., 2014. Integrated multicomponent solute geothermometry. Geothermics 51, 113–123. https://doi.org/ 10.1016/j.geothermics.2013.10.012.
- Taran, Y.A., Peiffer, L., 2009. Hydrology, hydrochemistry and geothermal potential of El Chichón volcano-hydrothermal system, Mexico. Geothermics 38 (4), 370–378.
- Tassi, F., Martinez, C., Vaselli, O., Capaccioni, B., Viramonte, J., 2005. Light hydrocarbons as redox and temperature indicators in the geothermal field of El Tatio (northern Chile). Appl. Geochem. 20 (11), 2049–2062.
- Tassi, F., Aguilera, F., Darrah, T., Vaselli, O., Capaccioni, B., Poreda, R.J., Delgado Huertas, A., 2010. Fluid geochemistry of hydrothermal systems in the Arica-Parinacota, Tarapacá and Antofagasta regions (northern Chile). J. Volcanol. Geotherm. Res. 192, 1–15.
- Truesdell, A.H., Nathenson, M., Rye, R.O., 1977. The effects of subsurface boiling and dilution on the isotopic compositions of Yellowstone thermal waters. J. Geophys. Res. 82 (26), 3694–3704.
- Trujillo, P., 1969. Estudio para el desarollo geotermico enel norte de Chile. Manifestaciones termales de El Tatio, Provencia de Antofagasta: CORFO Project Report.
- Trujillo, P., 1974. Catastro de recursos geotermicos de Chile. Seminario sobre los recursos energeticos de Chile. CONYCIT.
- Vakin, E.A., Pilipenko, G.F., 1986. The Mutnovsky geothermal area in Kamchatka. Exploration and Exploitation of Geothermal Resources in Volcanic Areas. Nauka, Moscow, Russia (36–45 pp.).
- Welhan, J.A., Fritz, P., 1977. Evaporation pan isotopic behavior as an index of isotopic evaporation conditions. Geochim. Cosmochim. Acta 41 (5), 682–686.
- Zeil, W., 1959. Das Fumarolen- und Geysir-Feld westlich der Vulkangruppe des Tatio (Provinz Antofagasta, Chile). Bayerische Akademie der Wissenschaften, Abhandlung der Mathematisch-Naturwissenschaftliche Klasse, Muenchen, Deutschland, p. 22 (n. 96).